GEOPHYSICS, VOL. 44, NO. 6 (JUNE 1979); P. 1097–1115, 15 FIGS.



# Microseisms in geothermal exploration—studies in Grass Valley, Nevada

Alfred L. Liaw* and T. V. McEvilly‡

Frequency($f$)-wavenumber($k$) spectra of seismic noise in the bands $1 \leq f \leq 10$ Hz in frequency and $|k| \leq 35.7$ cycles/km in wavenumber, measured at several places in Grass Valley, Nevada, exhibit numerous features which can be correlated with variations in surface geology and sources associated with hot spring activity. Exploration techniques for geothermal reservoirs, based upon the spatial distribution of the amplitude and frequency characteristics of short-period seismic noise, are applied and evaluated in a field program at this potential geothermal area.

A detailed investigation of the spatial and temporal characteristics of the noise field was made to guide subsequent data acquisition and processing. Contour maps of normalized noise level derived from judiciously sampled data are dominated by the hot spring noise source and the generally high noise levels outlining the regions of thick alluvium. Major faults are evident when they produce a shallow lateral contrast in rock properties. Conventional seismic noise mapping techniques cannot differentiate noise anomalies due to buried seismic sources from those due to shallow geologic effects. The noise radiating from a deep reservoir ought to be evident as body waves of high-phase velocity with time-invariant source azimuth. A small two-dimensional (2-D) array was placed at 16 locations in the region to map propagation parameters. The $f$-$k$ spectra reveal shallow local sources, but no evidence for a significant body wave component in the noise field was found.

With proper data sampling, array processing provides a powerful method for mapping the horizontal component of the vector wavenumber of the noise field. This information, along with the accurate velocity structure, will allow ray tracing to locate a source region of radiating microseisms. In Grass Valley, and probably in most areas of sedimentary cover, the 2–10 Hz microseismic field is predominantly fundamental-mode Rayleigh waves controlled by the very shallow structure.

## INTRODUCTION

Two methods have been proposed to utilize microseisms for delineating geothermal reservoirs. The first is based on the speculation that hydrothermal processes deep in the reservoir radiate seismic wave energy in the frequency band 1 to 100 Hz. If this phenomenon exists, the exploration method becomes a rather straightforward "listening" survey, using stations on a 0.5- to 2-km grid. Contours of noise power on the surface should delineate noise sources. This is the "standard" noise survey used widely in geothermal exploration. A second approach interprets the noise field as propagating elastic waves of appropriate type, e.g., fundamental-mode Rayleigh waves, and inverts their propagation characteristics to obtain the distribution of medium properties, i.e., velocity and attenuation, both laterally and vertically. The propagation parameters of ambient microseisms

Presented at the 46th Annual International SEG Meeting October 28, 1976 in Houston, Texas. Manuscript received by the Editor July 19, 1977; revised manuscript received November 10, 1978.
*Res. and Dev. Dept., ARCO Oil and Gas Co., P.O. Box 2819, Dallas, TX 75221; formerly Engineering Geoscience, University of California, Berkeley, CA 94720.
‡Seismograph Station, Dept. of Geology and Geophysics, University of California, Berkeley, CA 94620.

so measured will also locate distinctive radiation sources. With sufficient knowledge of the wave nature of the microseisms and a reasonably accurate velocity-depth model, a fixed nonaliased array can be used in a beam-steering mode to define the source region of radiated noise. Both approaches, as used in typical surveys, suffer greatly when data are contaminated by nongeothermal seismic noise, by interfering seismic wave trains, or by improper temporal and spatial data sampling. These pervasive problems have combined to render noise analysis at best a qualitative geophysical method and have substantially limited the acceptance of the seismic noise survey as an integral element in geothermal exploration.

This study attempts to avoid such problems through careful analysis of microseismic data in an evaluation of the feasibility of ground noise studies in geothermal site delineation. We report a series of investigations undertaken near Leach Hot Springs in Grass Valley, within the region of generally high heat flow in northern Nevada. We first quantify the spatial and temporal variations of ground noise in the region and find that the seismic noise spectrum is strongly affected by near-surface sedimentary layers at the recording site. In fact, with broadband seismic sensors in a mapping technique using amplitudes and frequencies, one can outline lateral variations in alluvial thickness. This standard mapping technique cannot differentiate noise enhancement due to shallow structure from noise enhancement due to a buried seismic source. On the other hand, we find that the mapping of wave propagation parameters provides additional information about the noise field. However, the successful application of this technique requires some understanding of the wave nature of microseisms. We used multiple-sensor arrays to study the seismic coherency as a function of frequency and spatial separation. Based on this information, an array was designed to record propagating microseismic data. The array data were processed by both the frequency domain beamforming method (BFM) and the maximum-likelihood method (MLM). From the dispersion curves obtained in the array study, it was verified that the seismic noise consists primarily of fundamental-mode Rayleigh waves.

This paper consists of several sections describing the methodology, the area studied, the data, its interpretation, and recommendations. This study together with other detailed geologic, geochemical, and geophysical studies carried out in the area provide all the ingredients, except the test wells, for a complete case history on a geothermal prospect.

## GEOTHERMAL GROUND NOISE

Clacy (1968) first suggested that seismic noise increased near geothermal reservoirs. His first results northeast of Lake Taupo, New Zealand, were based on contours of total noise amplitude in the frequency band of 1 to 20 Hz. In subsequent surveys at Wairakei, Waiotapu, and Broadlands geothermal areas, he found that the local noise amplitude anomalies were characterized by a dominant frequency of 2 Hz, whereas, away from the area of the anomaly, frequencies higher than 3 Hz predominated. On the other hand, Whiteford (1970) found in repeat surveys of the same areas that neither the shape of the frequency spectrum nor its dominant frequency conformed to any regional pattern. Whiteford measured the absolute ground motion in the Waiotapu geothermal area and found that, within a distance of 1 to 2 km of the high heat flow area, the average minimum ground particle velocity was greater than $150 \times 10^{-9}$ m/sec, while farther away the amplitude of the ground movement decreased by a factor of about 3 and, in addition, exhibited pronounced diurnal variations.

In the United States, a similar survey was first carried out southeast of the Salton Sea by Goforth et al (1972) who suggested for geothermal reservoirs an empirical relationship between high-temperature gradient and high seismic noise level. Their results showed a significant increase in the noise power in the frequency band of 1 to 3 Hz at sites above the reservoir. They estimated the power spectrum at each site from ten 200-sec data segments taken over eight hours of nighttime recording. The contour map of the total power in the frequency band of 1 to 3 Hz was similar to the temperature gradient contour map. Douze and Sorrells (1972) conducted a similar survey over the nearby East Mesa area, where they found that the total seismic power in the 3 to 5 Hz band exhibited spatial variations similar, in general, to gravity and heat flow fields. East Mesa was later surveyed by Iyer (1974) with significantly different results. Iyer measured seismic noise by averaging 20 of the lowest values of the root-mean-square (rms) amplitude in several narrow frequency bands, using data blocks of 81.92 sec selected from four hours of digital data. He did not find an anomaly in seismic noise associated with geothermal activity but only the noise from canals and freeway traffic.

The seismic pulsation associated with several geysers in Yellowstone National Park is believed to be indicative of the heating of water in the underground reservoir and the eruption triggered by the

superheated system. Nicholls and Rinehart (1967) have studied the seismic signature of several geysers in the park and inferred that their predominant pulse frequencies are quite similar, in the range of 20–60 Hz, presumably due to steam action. The very low-frequency seismic pulses recorded at Old Faithful, Castle, Bead, Plume, and Jewel geysers are believed to be associated with some type of water movement. The maximum amplitude of seismic pulses recorded in Yellowstone Park is $5.08 \times 10^{-5}$ m/sec. At Old Faithful Geyser, the maximum amplitude is $2.54 \times 10^{-5}$ m/sec at 30–50 Hz.

Iyer and Hitchcock (1974) also found good correlation between geothermal activity and high seismic noise levels in the 1 to 26 Hz range in the Park. The ground noise level in nongeothermal areas of the Park is approximately 13 to $15 \times 10^{-9}$ m/sec at 1 to 26 Hz. In the Lower and Upper Geyser Basins where there are numerous geysers and hot springs, the average noise level is in general higher than $50 \times$

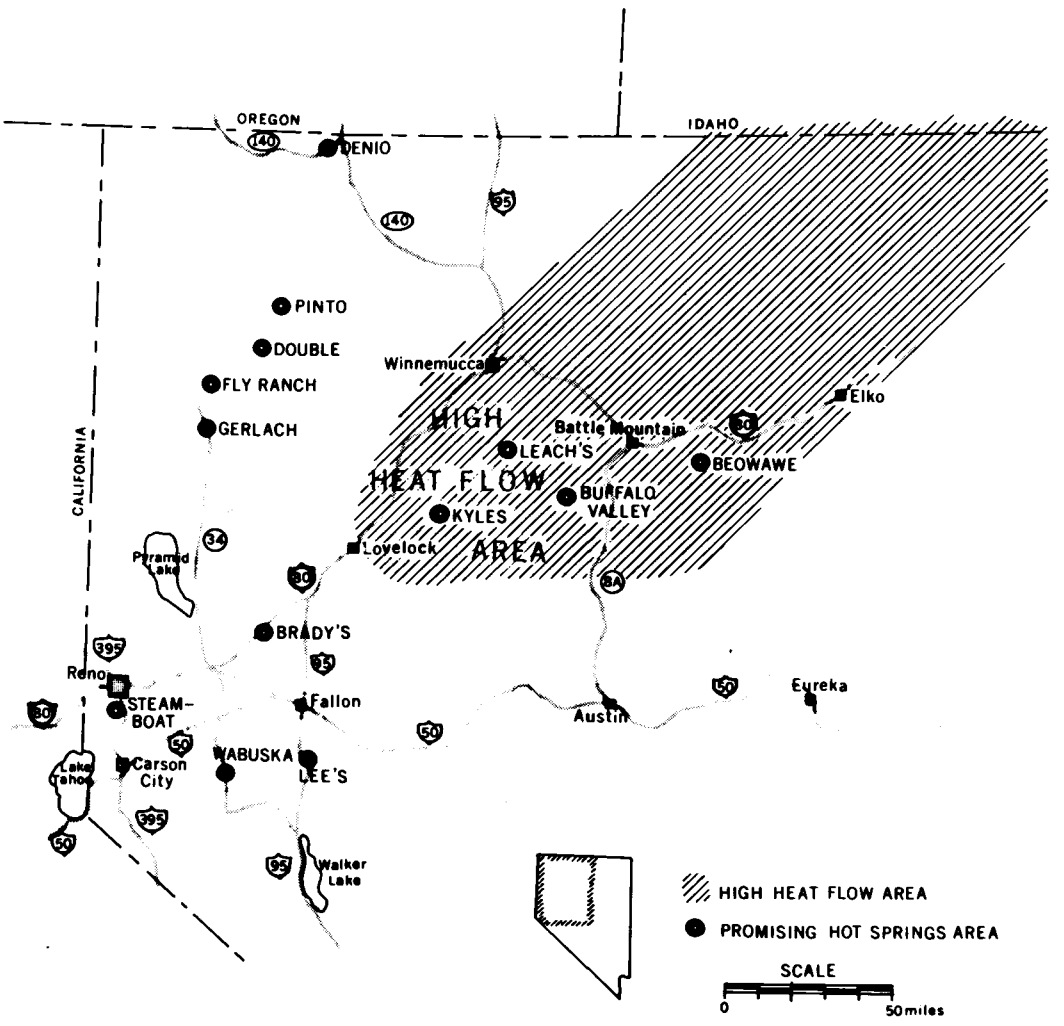


FIG. 1. Prominent thermal springs areas and the Battle Mountain high heat flow region in Northwestern Nevada. Shaded area indicates high heat flow area.

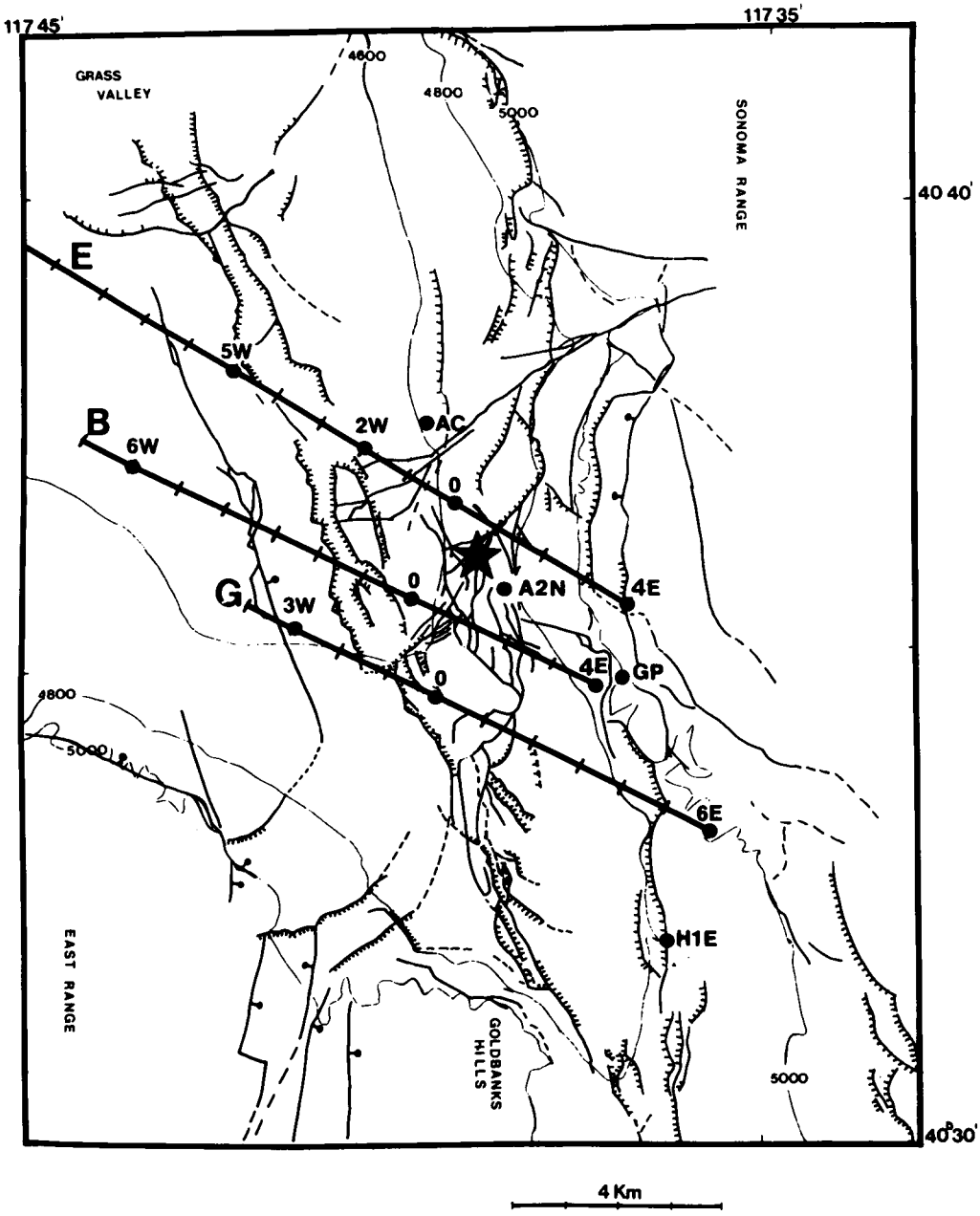


FIG. 2. Mapped faults and pertinent geophysical traverses in the Leach Hot Springs area. Hachured lines indicate down-faulted sides of scarplets; ball symbols indicate downthrown side of other faults. Star shows location of Leach Hot Springs. Heavy solid lines are survey lines E, B, and G with tick marks every 1 km.

$10^{-9}$ m/sec and reaches a value of $672 \times 10^{-9}$ m/sec near Old Faithful. In the Norris Basin, another highly active geyser basin in the Park, the noise level varies from 50 to $500 \times 10^{-9}$ m/sec. Part of the observed noise in the Lower, Upper, and Norris Geyser Basins is no doubt generated by the hydrothermal activity at the surface. The measurements near Old Faithful indicate that high-frequency noise, in the 8 to 16 Hz band, is generated during geyser eruptions; the noise level of lower frequencies is not affected by the eruption cycles. Noise levels around Mammoth Hot Springs are two to five times higher than in the surrounding area. There is no geyser or fumarole here, and the geothermal water is relatively cooler than at Norris and the other geyser basins. Hence, it is very unlikely that the seismic noise observed here is generated near the surface. The noise anomaly observed in the area between Lower Falls and Mud Volcano could be caused by ground amplification effects in the soft sedimentary deposits.

Correlations have also been reported between geothermal activity and high seismic ground noise in the Vulcano Islands, Italy (Luongo and Rapolla, 1973), the Coso geothermal area, China Lake, California (Combs and Rotstein, 1975), and Long Valley, California (Iyer and Hitchcock, 1976). High-frequency noise ($f > 8$ Hz) in the vicinity of geysers, fumaroles, and hot springs is associated with hydrothermal activity near the surface and during the geyser eruption. Low-frequency noise ($f < 8$ Hz) is not affected by geyser eruption cycles and is probably generated at depth.

It is evident that a noise power anomaly may result not only from an active seismic source, but also from lateral variation in near-surface velocity, particularly where low-velocity alluvium is involved. In order to identify a buried radiating source, the direction of propagation and the apparent phase velocity of the coherent noise field must be utilized. Whiteford (1975) successfully located the noise source in the Wairakei area using tripartite geophone array measurements. Iyer and Hitchcock (1976) used an L-shaped array with 106-m geophone spacing in Long Valley and found that propagation azimuths for the high-velocity waves defined the area of surface geothermal phenomena, but they found that random directions of propagation were characteristic of low-velocity waves.

Azimuth and apparent velocity measurements are complicated for microseisms because of multipath arrivals and nonstationary characteristics. In addition, very short wavelengths (10–20 m) can characterize the noise field in areas of low-velocity surface materials, and these are often aliased to lower wavenumber (longer wavelengths, higher velocities) and misinterpreted if array geophone spacing is too large.

## MICROSEISMS

The study of microseisms, or earth noise, has been directed primarily toward frequencies less than 0.5 Hz, where the source is either ocean waves associated with storms (Longuet-Higgins, 1950; Gutenberg, 1958; Oliver, 1962; Oliver and Ewing, 1957; Oliver and Page, 1963; Haubrich and Mackenzie, 1965; Haubrich and McCamy, 1969; Fix, 1972) or atmospheric disturbances (Sorrells et al, 1971; Savino et al, 1972). Background microseism spectra for the range 0.02 to 1 Hz are characterized by two maxima at frequencies near 0.071 and 0.143 Hz (periods of 14 and 7 sec), both apparently due to coastal storm effects. In the period range beyond about 3 sec, local atmospheric pressure changes contribute primarily to the microseisms observed.

High-frequency microseisms ($f > 0.5$ Hz) observed away from the coast are generated locally by cultural activity, traffic, wind, rivers (Wilson, 1953; Robertson, 1965; Iyer and Hitchcock, 1974), by geothermal processes, and by distant sources (Lacoss et al, 1969). Noise observed at the ground surface usually consists principally of fundamental-mode Rayleigh waves. At depths where the fundamental mode has decreased to negligible amplitude, the noise consists of Rayleigh modes of order higher than third, or of body waves (Douze, 1967). Sharp spectral peaks and troughs can be related to shallow geologic structure. Low-velocity alluvium or weathering can produce a significant amplitude increase of seismic noise over that observed at a bedrock site. Thus, the shallow section can provide a waveguide for microseisms at particular frequencies (Kanai and Tanaka, 1961; Sax and Hartenberger, 1965; Katz, 1976; Iyer and Hitchcock, 1976). Certain sources of microseisms, such as waterfalls or pipelines, can produce narrow-band radiation. Near the Owens River at Long Valley, California, Iyer and Hitchcock (1976) report that the flowing river generates noise at frequencies above 6 Hz, attenuated by about 12 dB at 1 km from the river. At East Mesa, California, the canals seem to be continuous wide-band sources of seismic noise which drops off rapidly with distance, reaching a fairly steady level at 3 km. At the power drops (small waterfalls) along the canal, however,

intense noise is seen in a narrow frequency band around 2.5 Hz (Iyer, 1974).

## AREA OF STUDY

Leach Hot Springs in Grass Valley, Nevada is located 30 km south of Winnemucca (Figure 1). Grass Valley is a typical valley of the Basin and Range province with normal faulting, major earthquakes, and hot springs occurring along the valley margins. The valley is bounded by the Sonoma and Tobin Ranges to the east and the basalt-capped East Range to the west. The valley narrows south of the hot springs as it approaches the Goldbanks Hills (Figure 2). These ranges are composed of Paleozoic sedimentary rocks or Triassic siliceous clastic and carbonate rocks. Some granitic intrusions, probably of

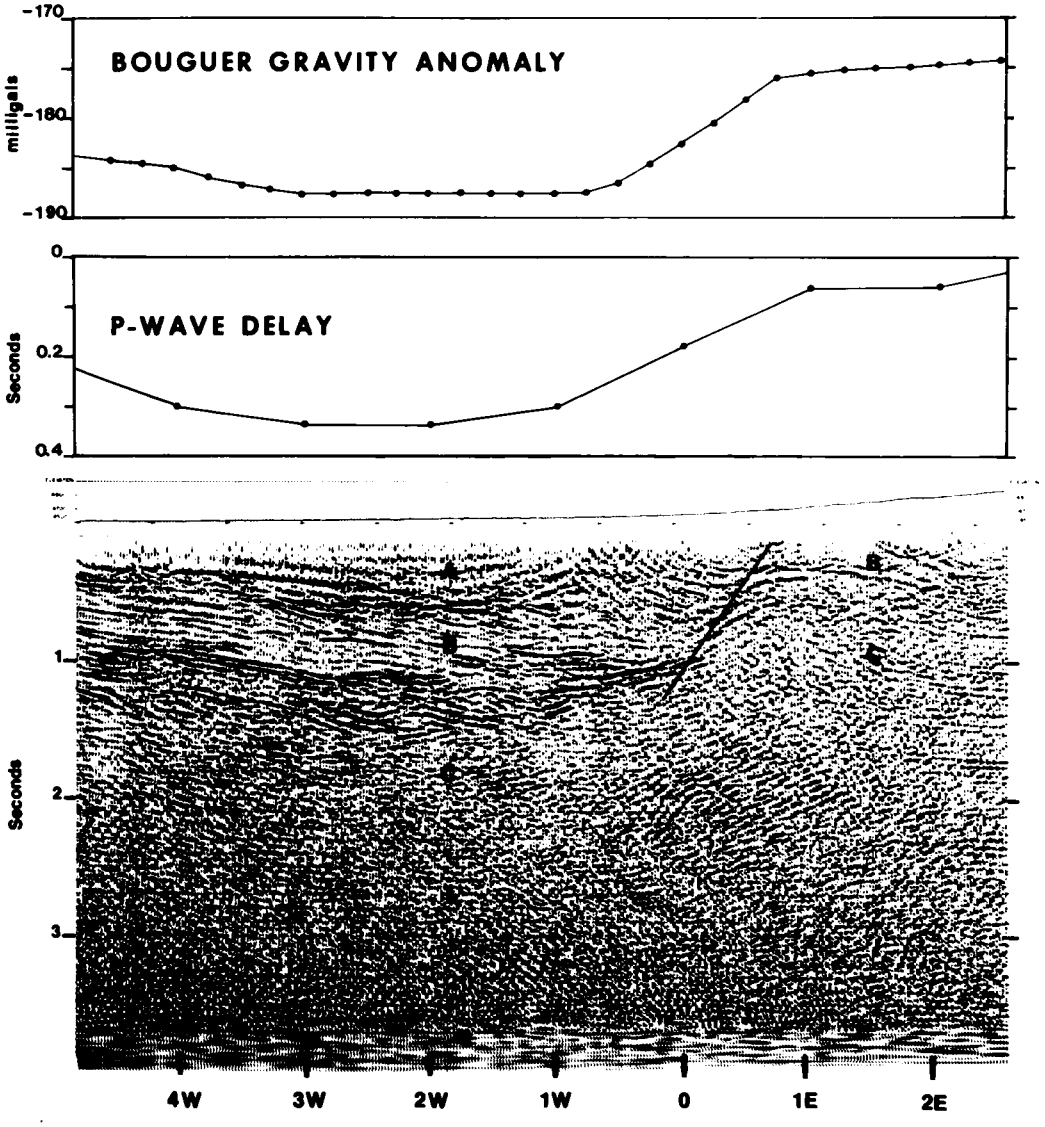


FIG. 3. Profiles for line E, 5W to 3E, of Bouguer gravity anomaly, *P*-wave delay, and migrated seismic reflection section, showing east margin fault (trace at 1E) and maximum sediment thickness near 2W. Averaged section velocities are: (a) 1.8 km/sec, Quaternary alluvium; (b) 2.9 km/sec, Tertiary sediments; and (c) 4.0 km/sec, Paleozoic rocks.

Triassic origin, have offset rock units of several tens to several hundreds of meters measured vertically. As shown on the fault and lineament map (Figure 2), the present day hot springs occur at the intersection of a major northeast-trending fault and the more common north-northwest/south-southeast trending lineament on the eastern side of the valley.

Leach Hot Springs is within the high heat flow area of northern Nevada indicated in Figure 1. This high heat flow area is often called the "Battle Mountain high" (Sass et al, 1971) and exhibits heat flow values in the range of 1.5 to 3.5 HFU (1 HFU = 10 cal/m$^2$ sec). The diffuse region of elevated heat flow over the Basin and Range province is generally thought to be an expression of high temperature in the lower crust and upper mantle, and it seems reasonable to interpret the localized Battle Mountain high as an effect of fairly recent intrusion of magma into the earth's crust. Quaternary volcanism within the province supports this hypothesis.

Geophysical data were obtained primarily along 17 survey lines, although not all methods were employed on every line. Line E (Figure 2) is typical. Bouguer gravity anomaly, $P$-wave delay data, and seismic reflection data, presented in Figure 3 for line E, indicate that the greatest thickness of sediments and major faulting occur near the eastern valley margin. The major lithologic units from the seismic reflection section are Quaternary alluvium (1.8 km/sec), Tertiary sedimentary and volcanic rocks (2.9 km/sec), Paleozoic rocks (4.0 km/sec), and deep basement (5.0 km/sec), respectively. The basement surface rises gently to the west but is apparently upthrown at the eastern boundary faults.

A low apparent resistivity zone beneath 2W–4W on Line E (Figure 2) (Beyer et al, 1976), found in the dipole-dipole resistivity survey, has been identified with Tertiary sediments. Since the heat flow value in this zone is not high by Battle Mountain standards (2.24 HFU), the accumulation of conductive sediments, such as ancient playa deposits in the deepest portion of the valley, is probably responsible for the resistivity anomaly. More details of the geophysical data obtained in the Grass Valley area are given by Beyer et al (1976).

## DATA ACQUISITION AND PROCESSING

A portable seismic network, with up to 12 stations linked by radio telemetry to a recording system mounted in a small, two-wheeled trailer, was designed for simplicity, flexibility, and ease of installation. It proved possible for two men to deploy the sensors and test the telemetry in about one day. Ease of network emplacement made it possible to modify the array as data were collected and to design field experiments with multiple objectives.

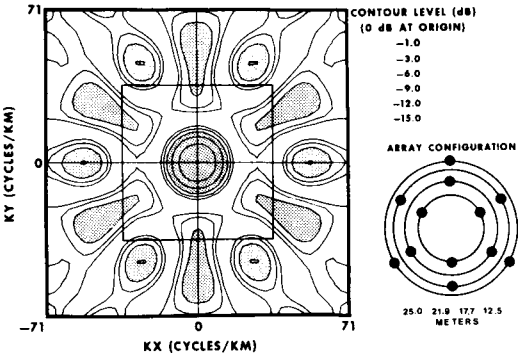


FIG. 4. Array configuration and its contoured impulse response in wavenumber space, plotted to $k_x$ and $k_y = 71$ cycles/km. The effective Nyquist wavenumber can be seen to vary with azimuth in the range of approximately 50–70 cycles/km. The interior square outlines the standard wavenumber plot range of 35.7 cycles/km used in subsequent figures. Radii of the array concentric circles are given.

A 4.5-Hz vertical-component geophone, a high-gain amplifier (60–120 dB), a voltage controlled oscillator, and a radio transmitter constituted the station site equipment. A 0.1-watt transmitter gave a range of about 20 km for average topography. In applications using all 12 geophones spaced over a small aperture array (50-m diameter), the radio links were eliminated and signals were transmitted by cable to the recording trailer. The trailer housed the radio receivers, FM discriminators, a 14-channel slow-speed FM tape recorder (0.12 ips, 0–40 Hz; or 0.24 ips, 0–80 Hz), timing system, and batteries. A slow-speed smoked-paper recorder was used as a monitor. The system had about 40 dB dynamic range (peak-to-peak measurement), limited primarily by the tape recorder.

To study the spatial variations of ground noise amplitude, we occupied a reference site at E2W (line E, station 2W in Figure 2) throughout the survey period. Normally we recorded overnight, with stations spaced at 1-km intervals along the survey lines. The smoked-paper monitor record was observed every morning to verify the occurrence of low seismic noise level at the reference site; otherwise, the sites were reoccupied another night, until low-noise conditions prevailed. Geophones were buried about one

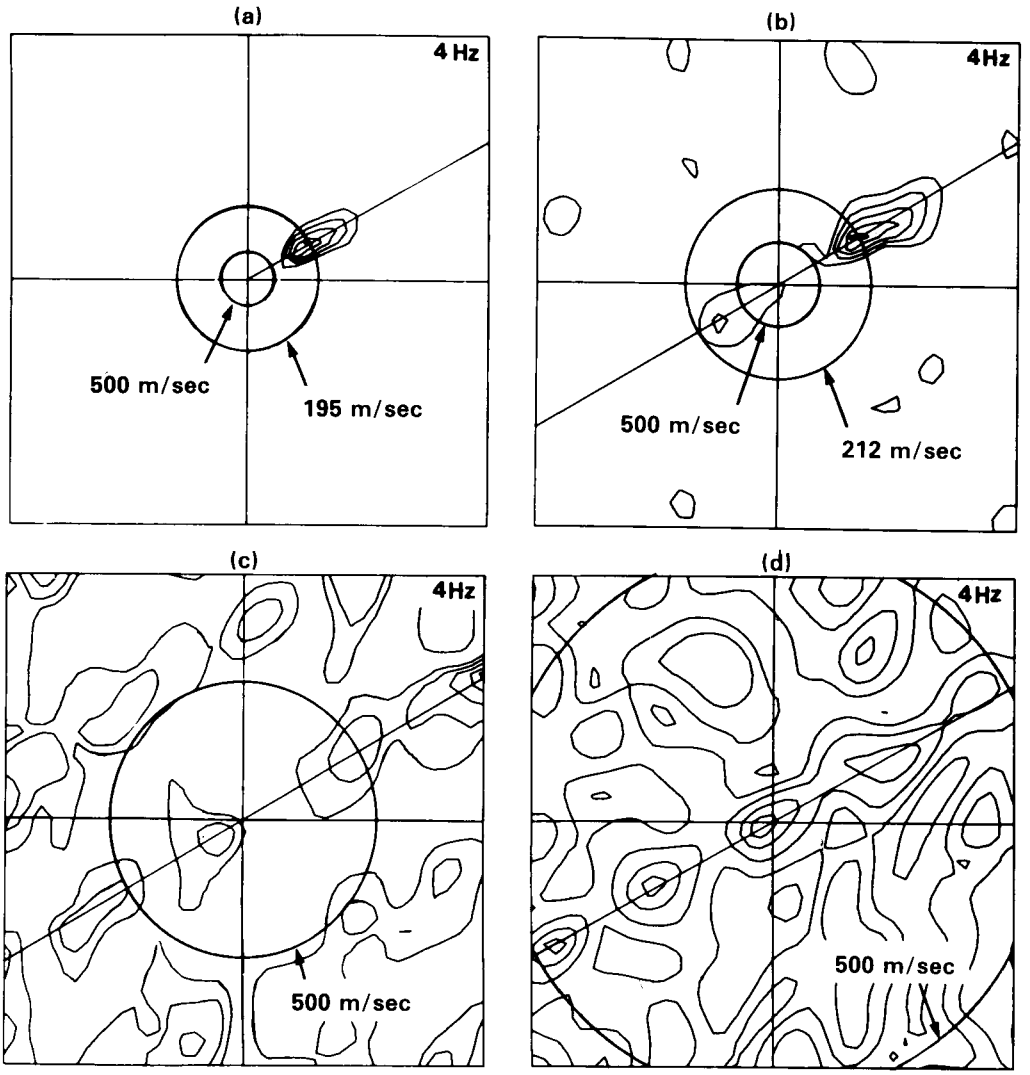


FIG. 5. High-resolution $f$-$k$ power spectral density estimates for a simulated 4-Hz plane wave signal propagating N60°E across the array at phase velocity 200 m/sec ($k$ = 20 cycles/km) to illustrate spatial aliasing. The array configuration is as shown in Figure 4, with dimensions scaled (a) 1, (b) 1.5, (c) 5, and (d) 10 times the radii values indicated in Figure 4. The maximum $k_x$ and $k_y$ values in the plots are (a) 71.4, (b) 47.6, (c) 14.3, and (d) 7.1 cycles/km corresponding approximately to the effective Nyquist wavenumbers for the arrays. The $f$-$k$ power spectral density contours are −1.0, −3.0, −6.0, −9.0, and −12.0 dB below the main peak. Circles indicate the constant velocities shown, expanding with array size. Aliasing is apparent in the high phase velocities in (b), (c), and (d), easily misinterpreted as detected body waves.

foot below the surface. Before and after a survey, all geophones were buried in a common hole to verify uniformity of their responses.

For determination of spatial variation of wavenumber, an array of 12 closely spaced geophones was emplaced at a site each evening. Data were transmitted by cable to the recording vehicle some 500 m from the array. The array configuration and its impulse response in wavenumber space are shown in Figure 4. The existence of short-wavelength noise components and the low coherence seen at large geophone separation both dictated the tight array spacing used. An array of 100-m element separation or more, commonly used in ground noise studies elsewhere, would give spurious results because spatial aliasing folds the high-wavenumber noise components (which we have seen dominant in the valley alluvium) into low-wavenumber noise components. The spatial aliasing results in the appearance of erroneously high-velocity ground noise, which is interpreted as body waves. The effect of spatial aliasing due to inadequate element separation is illustrated in Figure 5, where we processed a simulated 4 Hz plane wave with 50-m wavelength, propagating with phase velocity of 200 m/sec in the direction N60°E across four arrays. Those arrays have identical array shapes and numbers of sensors but different sensor spacing. The diameters of the arrays are 50, 75, 250, and 500 m, such that the sensor spacing for each array is proportional to the array size. Since the plane waves are propagating at an azimuth of 60 degrees, the folding effects are evident along the directions of 60 degrees and 240 degrees. Many interpretations of microseisms as body waves, based on coarse sensor separation, may well be incorrect due to aliased low-velocity surface waves as seen, for example, in Figure 5c. It is true, of course, that when the array is made small enough to accommodate the short-wavelength noise characteristics, resolution for near-vertically incident body waves is degraded seriously; however, they could be enhanced by appropriate array expansion and spatial filtering.

For determination of the spatial variation of amplitude, data were selected judiciously from the quietest recording period in the early morning hours. At least 28 simultaneously recorded blocks of data were chosen from each of the recording stations, avoiding any spurious transient signals. Each data block of 12.8 sec length was filtered and digitized. The resulting 512-point records were tapered to zero at each end over 51 points and Fourier transformed. The Fourier transform was multiplied by its complex conjugate to produce power spectral density. The estimated power spectral density at each location is the average over at least 28 data blocks, to increase statistical confidence. The ground velocity spectral density (VSD) in $m\mu/sec/\sqrt{Hz}$ was obtained by taking the square root of the power spectral density estimate and correcting it for system response. The relative intrinsic noise level, in dB, for a particular frequency band at a station is obtained by integrating the velocity spectral density over the frequency band and normalizing by that quantity at the reference station.

For estimation of the frequency($f$)-wavenumber ($k$) power spectral density, array data were processed by using both the frequency domain beam-forming method (BFM) (Lacoss et al, 1969) and the maximum-likelihood method (MLM) (Capon, 1969). The BFM estimates $f$-$k$ power spectral density by the formula

$$\hat{P}(f,\mathbf{k}) = \frac{1}{N^2}\,\mathbf{a}'\cdot\hat{\mathbf{S}}\cdot\mathbf{a}, \tag{1}$$

where $\hat{P}(f,\mathbf{k})$ is BFM $f$-$k$ power spectral density estimate, $N$ is the number of geophones in the array, $\mathbf{S}$ is the estimate of the coherent power spectral density matrix between sensors, and $\mathbf{a}'$, the conjugate transpose of $\mathbf{a}$, is given by

$$[\exp(i2\pi\mathbf{k}\cdot\mathbf{r}),\ \exp(i2\pi\mathbf{k}\cdot\mathbf{r}_2),\ \ldots,\ \exp(i2\pi\mathbf{k}\cdot\mathbf{r}_N)], \tag{2}$$

where $\mathbf{r}_n$ is the coordinate of the $n$th geophone location. Each entry of $\hat{\mathbf{S}}$, $\hat{S}_{ln}(f)$, is obtained from

$$S_{ln}(f) = \frac{1}{M}\sum_{m=1}^{M}\Phi_{lm}(f)\,\Phi^*_{nm}(f), \tag{3}$$

by the normalization

$$\hat{S}_{ln}(f) = \frac{S_{ln}(f)}{\sqrt{S_{ll}(f)S_{nn}(f)}}, \tag{4}$$

where $\Phi_{lm}(f)$ are the Fourier coefficients of the $m$th block time series from the $l$th geophone, and * indicates complex conjugate.

BFM is commonly called a conventional method, whose operation can be seen by rearranging equation (1) to be

$$P(f,\mathbf{k}) = \frac{1}{N^2}\sum_{n=1}^{N}\sum_{l=1}^{N}\hat{S}_{ln}(f)\cdot \cdot\exp[-i2\pi\mathbf{k}\cdot(\mathbf{r}_l-\mathbf{r}_n)]. \tag{5}$$

For BFM, a uniform weighting function is applied

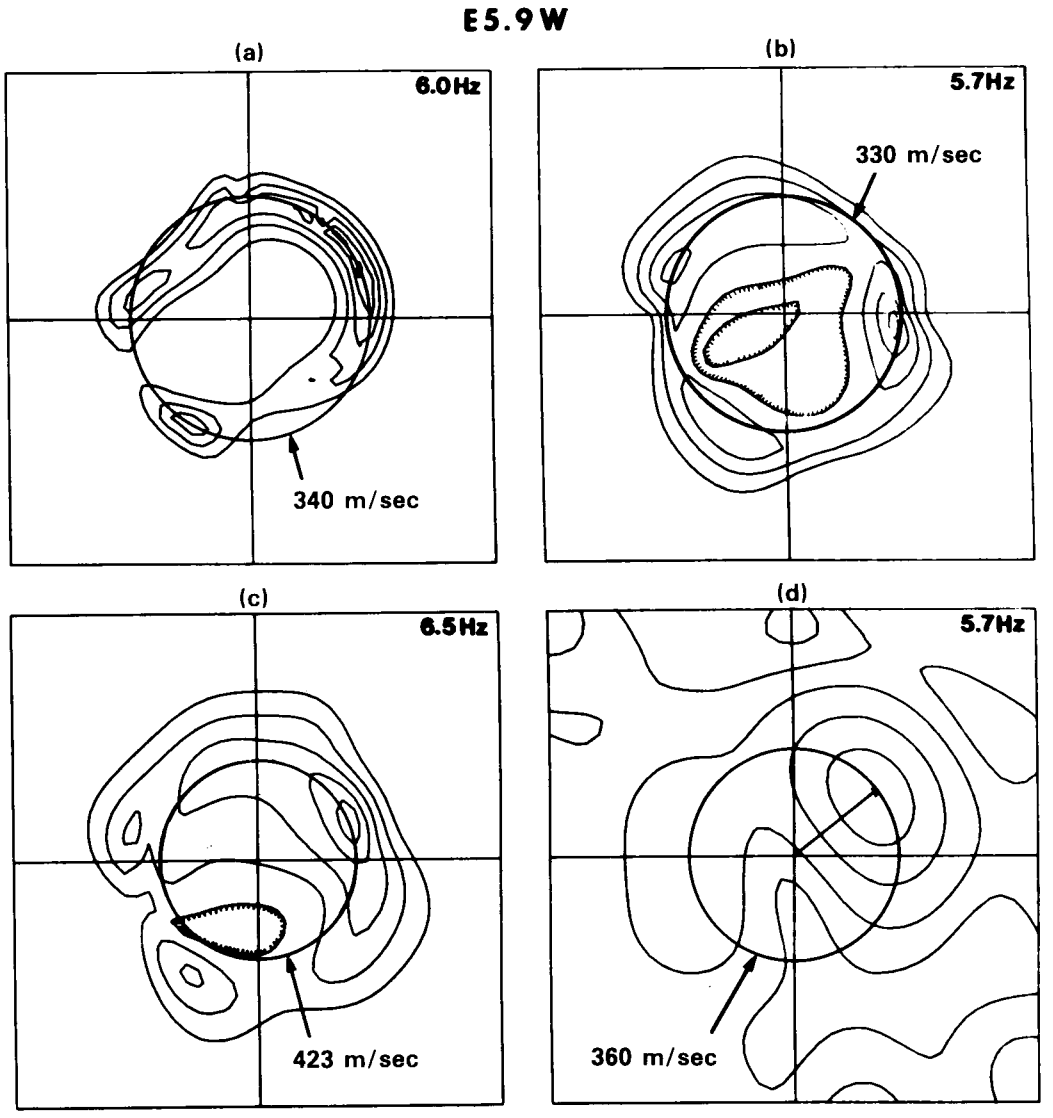


FIG. 6. Results of $f$-$k$ analysis for site E5.9W (line E, station 5.9W) for different data block lengths, comparing MLM and BFM: (a) 12 data blocks, each with 128 points, processed by MLM, (b) 24 data blocks, each with 64 points, processed by MLM, (c) 48 data blocks, each with 32 points, processed by MLM, (d) 24 data blocks, each with 64 points, processed by BFM. The frequency on each frame corresponds to a maximum $f$-$k$ power spectral density estimate. The range of wavenumber plotted is 35.7 cycles/km in both $k_x$ and $k_y$.

to each array element and then a delay-and-sum operation is performed. The resolution in wavenumber space is therefore strongly characterized by the impulse response of the array (Figure 4) with prominent side lobes. In the presence of multipath propagation, the large side-lobe effects are not clearly recognizable, resulting in an ambiguous pattern of peaks in wavenumber space with loss of resolution due to smearing of the true spectrum.

MLM, sometimes called the high-resolution method, calculates the $f$-$k$ power spectral density estimate by

$$\tilde{P}(f, \mathbf{k}) = (\mathbf{a}' \cdot \hat{\mathbf{S}}^{-1} \cdot \mathbf{a})^{-1}. \tag{6}$$

To motivate this operation, equation (6) can be written as

$$\begin{aligned}\tilde{P}(f, \mathbf{k}) &= \sum_{l=1}^{N} \sum_{n=1}^{N} A_l(f, \mathbf{k}) A_n^*(f, \mathbf{k}) \hat{S}_{ln}(f) \cdot \\ &\quad \cdot \exp[-i2\pi \mathbf{k} \cdot (\boldsymbol{\ell} - \mathbf{r}_n)] \\ &= \frac{1}{M} \sum_{m=1}^{M} \left| \sum_{l=1}^{N} A_l(f, \mathbf{k})\, \Phi_{lm}(f) \cdot \right. \\ &\quad \left. \cdot \exp[-i2\pi \mathbf{k} \cdot \mathbf{r}_l] \right|^2, \end{aligned} \tag{7}$$

where $A_l(f, \mathbf{k})$ are optimal complex weighting functions, known as maximum-likelihood filters, applied to each sensor's output. The procedure for finding $A_l(f, \mathbf{k})$ involves the inversion of the signal-plus-noise coherent power spectral matrix, such that

$$A_l(f, \mathbf{k}) = \frac{\sum_{n=1}^{N} q_{ln}(f, \mathbf{k})}{\sum_{n=1}^{N} \sum_{l=1}^{N} q_{ln}(f, \mathbf{k})} \tag{8}$$

and $[q_{ln}(f, \mathbf{k})]$ is the inverse of the matrix $\{\hat{S}_{ln}(f) \exp[-i2\pi \mathbf{k} \cdot (\mathbf{r}_l - \mathbf{r}_n)]\}$. Application of the maximum-likelihood filters allows the array processor to pass an undistorted monochromatic plane wave with a given velocity corresponding to a peak in $f$-$k$ power spectral density and to suppress, in an optimal least-squares sense, the power of waves traveling at different velocities. The MLM impulse response, without noise, is ideally sharp; with noise, it depends on the characteristics of the data.

Theoretically, MLM has a disadvantage relative to BFM in terms of its sensitivity to measurement errors, especially in a case of channel mismatch (Cox, 1973). Mismatch may result from distortion in the waveform during propagation, or from amplitude, phase, and position errors in the sensors (geophones), sampling, and digitization. However, MLM spectra from the array data of Grass Valley seldom showed evidence of serious degradation. Regarding resolution of two separate waves, BFM depends on the array impulse response, while MLM depends not only on array response but also on the signal-to-noise ratio (Cox, 1973).

The maximum entropy method (MEM) would theoretically provide higher resolution estimates than the above two methods. Unfortunately, this method is developed only for equally-spaced (Barnard, 1969) and nonuniform-spaced (McDonough, 1974) linear arrays. It appears that, at present, MLM is the best method for processing 2-D array data for high resolution in the presence of multipath interference, the normal situation in ground noise studies.

Data blocks without sporadic noise pulses (i.e., transient-free) from each of the 12 geophones of the array were selected for processing. The number and length of the data blocks were selected for resolution and statistical stability of the estimated power spectral density. A MLM comparison of different numbers and lengths, holding the total number of data points constant, is illustrated with the array data from the site E5.9W by processing the identical data in three different lengths. The results are shown in Figure 6a for 12 blocks × 128 points, in Figure 6b for 24 blocks × 64 points, and in Figure 6c for 48 blocks × 32 points. We find that the use of either 12 blocks × 128 data points, or 24 blocks × 64 data points provides adequate resolution in wavenumber space and realistic direction estimates, especially in situations of multipath propagation. In Figure 6, the $f$-$k$ power spectral densities are estimated at each of 41 × 41 grid points in a 2-D wavenumber space at a desired frequency component. The frequencies selected for processing are maxima in the power spectral density curves. The wavenumber of the peak value in the wavenumber plot, along with the frequency, provides the estimate of apparent phase velocity and the direction of propagation for the most coherent propagation in the data sample.

A comparison of BFM and MLM is provided in Figures 6b and 6d for the 24 block × 64 point case. The resolution improvement in MLM is quite apparent. Consequently, our processing method was normally MLM.

Based on these studies, data were processed for the Grass Valley area using the large network spacing for studying spatial variations in ground noise

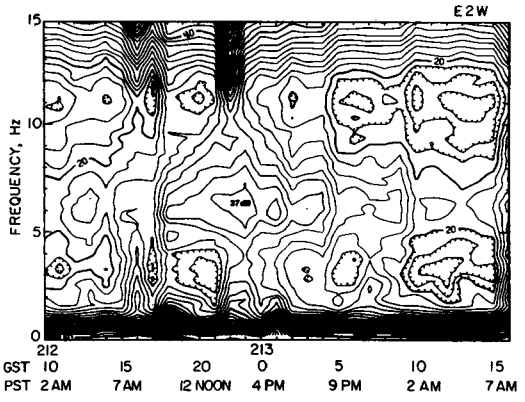


FIG. 7. Diurnal variation of ground noise level at reference site E2W, with respect to $10^{-11}$ m/sec/$\sqrt{\text{Hz}}$, (0 dB), from day 212, hour 10 to day 213, hour 16 of 1976. Contour interval is 2 dB. Note the minimum noise level at 2–4 AM for all frequencies.

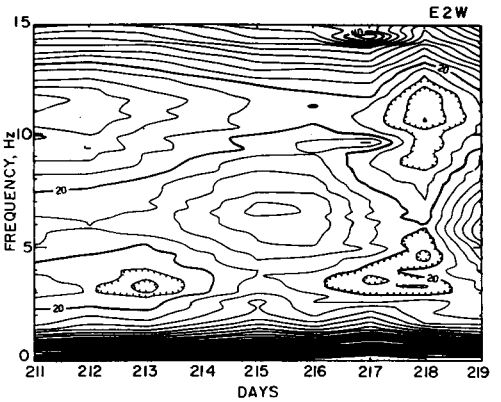


FIG. 8. Secular variation of early morning quiet ground noise level at E2W with respect to $10^{-11}$ m/sec/$\sqrt{\text{Hz}}$, (0 dB), from day 211 to day 219 of 1976. Contour interval is 2 dB. Thunderstorms and unsettled regional weather characterized days 214–216.

and utilizing the 25-m radius array with MLM for ground noise propagation ($f$-$k$) parameters.

## DATA AND INTERPRETATION

### Temporal variation of ground noise

The total seismic noise amplitude $\sigma(x, y, t, f)$ can be modeled very generally by

$$\sigma(x, y, t, f) = \sigma_i(x, y, t, f) + \sigma_m(x, y, t, f) + \sigma_l(x, y, t, f),$$

where

(1) $\sigma_i(x, y, t, f)$ is the intrinsic noise at the site, including geothermal noise,
(2) $\sigma_m(x, y, t, f)$ is the microseismic component from distant sources, and
(3) $\sigma_l(x, y, t, f)$ is the noise generated locally at the surface by human activity and atmospheric disturbances.

If we are interested only in intrinsic noise, the sampling and processing procedures must exclude the effect of the other two noise sources. To minimize local noise, $\sigma_l(x, y, t, f)$, the data must be taken between midnight and dawn, because normally the noise level is low. Figure 7 presents the diurnal variation of seismic noise at the reference site E2W. To construct this figure, transient-free noise data were chosen to estimate VSD every hour for a 30-hour period. Roughly 6 minutes of seismic noise actually went into each hourly average. The spectral density then was contoured as a function of time and frequency. The figure shows the typical wide-band, high-diurnal noise level, extending from 9 AM to 7 PM, the result of more disturbed daytime meteorological conditions and cultural activity in the area. This suggests that we record only between 2 and 4 AM to minimize contamination of the VSD estimate by unwanted diurnal noise sources.

A typical survey is carried out over a period of several days, so that long-term secular variations are apparent in the data. The nature of this variation over a 9-day period at the reference site E2W is shown in Figure 8. We estimate one VSD every 24 hours, using the quietest data during early morning hours, and contour the VSD from day 211 to day 219. In this figure, the high-amplitude seismic noise which appears from day 214 to day 216 is related to regional weather conditions. On those three days there were thunderstorms starting in the afternoon and ending in the early evening throughout the region. To eliminate temporal variations of the observed microseisms, the band-limited power of seismic noise at each site, obtained by integrating VSD over the frequency band of interest, is normalized by the simultaneous power in the same frequency band at the reference site, provided that data are sampled from the quiet period in early morning. Mapping the normalized power gives the spatial distribution of relative intrinsic noise power level.

### Spatial variation of ground noise

Estimation of ground noise VSD from simul-

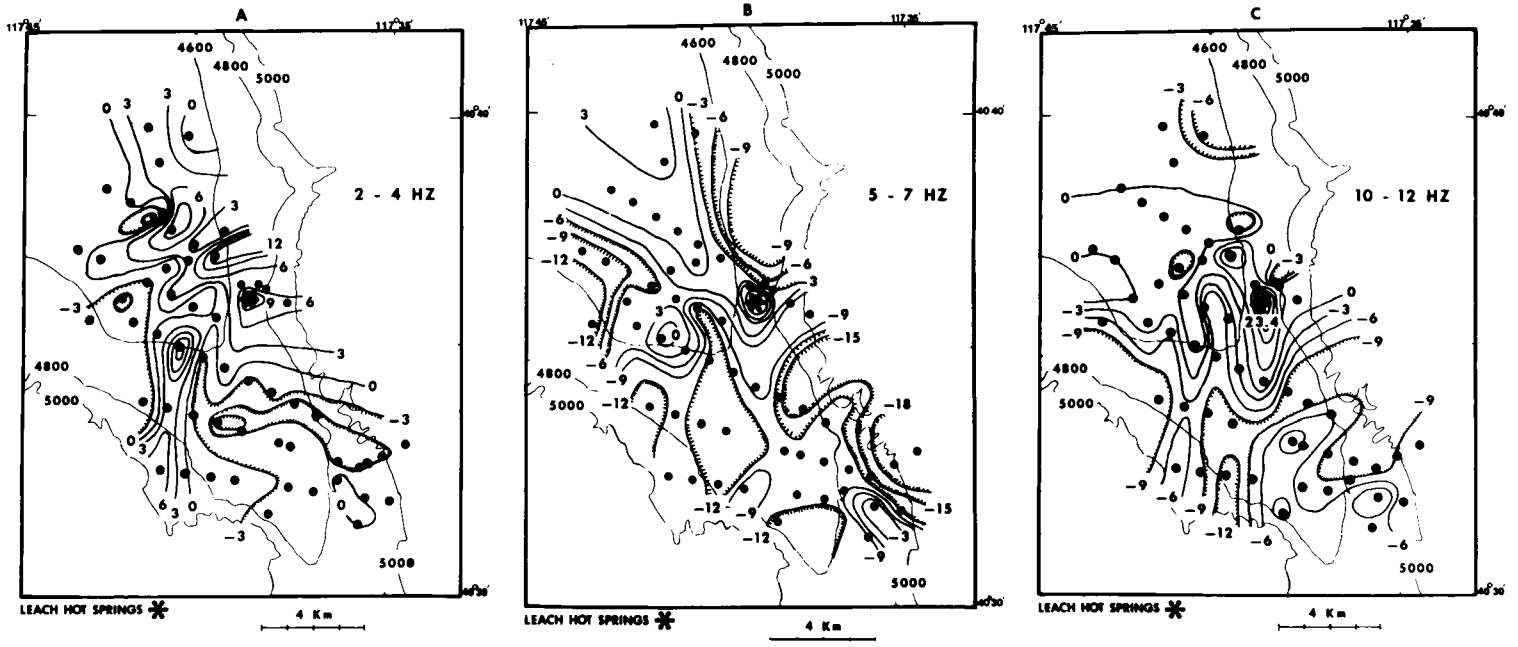


FIG. 9. Relative intrinsic noise power contours with respect to reference site E2W in three different frequency bands, namely (a) 2–4 Hz, (b) 5–7 Hz, and (c) 10–12 Hz. Contoured interval is 3 dB. Solid circles indicate geophone sites. Elevations are in feet. The star indicates Leach Hot Springs location.

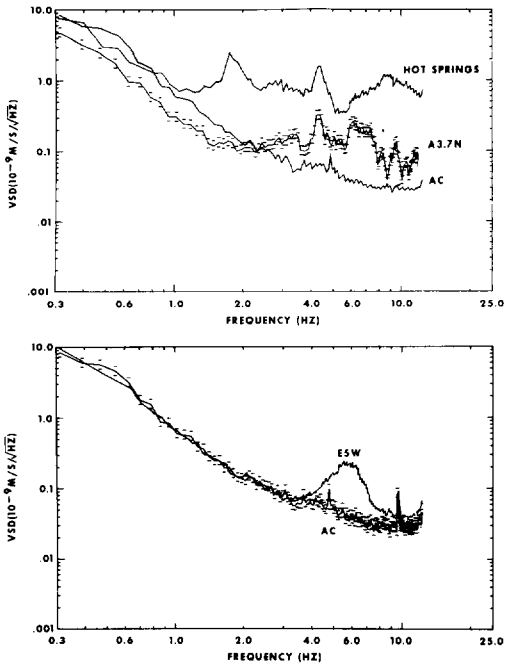


FIG. 10. Velocity spectral density (VSD) of ground noise at Leach Hot Springs and at site A3.7N, 500 m northwest of the hot springs (upper) and at site E5W in the center of the valley (lower) compared to bedrock site AC, at the valley edge (Figure 2). The horizontal bars show typical 95 percent confidence limits for A3.7N (upper) and AC (lower) sites.

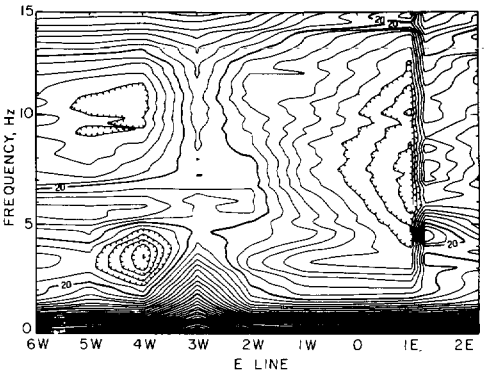


FIG. 11. Instantaneous noise field along survey line E. Abscissa is station location, with 1 km spacing and ordinate is frequency. Contour interval is 2 dB. Note high wide-band noise level at 3W, the region of thickest alluvial cover, and the sharp gradient across the valley margin fault trace at 1E.

taneous sampling in the early morning, with stations at 1-km intervals, yields relative intrinsic noise power contour maps as illustrated for the frequency band of 2–4 Hz (Figure 9a), 5–7 Hz (Figure 9b), and 10–12 Hz (Figure 9c). High noise levels are found at Leach Hot Springs and near the center of Grass Valley, as anticipated, but there are also local anomalies such as in the areas around G2W and G3W, H1E and H2E (see Figure 2 for site locations). Those ground noise anomalies, especially in the 5–7 Hz band, correlating spatially with the occurrence of Bouguer gravity anomalies, imply the occurrence of thickest alluvial deposits. The long-term stability of these anomalies is reproducible as indicated by close agreement with the results of a preliminary survey carried out in the summer of 1975, a year earlier than the survey for the data shown here.

Leach Hot Springs clearly generates seismic noise, but the noise is localized and does not propagate unattenuated more than a few km. In the vicinity of the springs, noise spectra show the high-amplitude seismic noise over a wide-frequency band; 500 m northwest of the hot springs (A3.7N) the amplitude of the noise at all frequencies greater than 1 Hz has attenuated nearly 20 dB. The noise spectrum at the Hot Springs site, at site A3.7N (500 m northwest of the Hot Springs site), and at a bedrock valley edge site AC (Figure 2) are shown in Figure 10. Note the wideband nature of the hot springs noise.

In the valley center, station E5W, the noise has a distinctive broad peak around 5.5 Hz, as can be seen at the bottom of Figure 10. The character of the broad valley peak varies from site to site, probably as a consequence of changes in near-surface properties. In Figure 9b, the areas of high-amplitude seismic noise in the 5–7 Hz band generally correspond to the areas of thick alluvium. The details of noise variation across the valley are illustrated by data for three typical survey lines, E, B, and G, shown respectively in Figures 11, 12, and 13.

The instantaneous ground noise level along 8.25 km of line E is presented in Figure 11. Data blocks were taken simultaneously from sites at E6W, 5W, 4W, 3W, 2W, 1W, 1E, 1.25E, and 2.25E. In this figure there is a clear peak at 5.5 Hz extending westward. The source of this well defined and band-limited peak is not clearly understood, though it is doubtless related to near-surface properties and is a surface wave with a wavelength of about 50 m. A wide-band ridge of rather high-amplitude noise appears at E3W and is frequently seen to extend to 1W. Maximum thickness of alluvium and the lowest

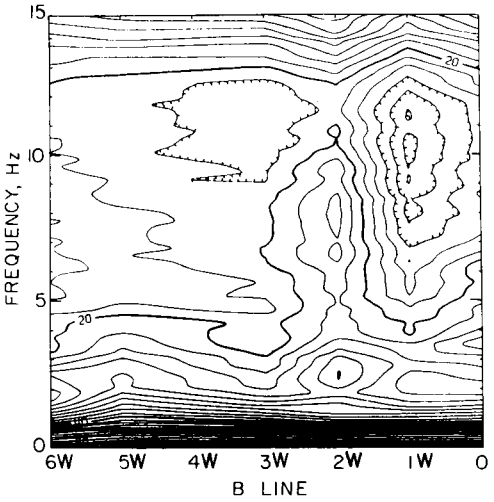


FIG. 12. Instantaneous noise field along survey line B. Abscissa is station location with 1 km spacing and ordinate is frequency. Contour interval is 2 dB. Note high wide-band noise level at valley center near 2W. Sharp gradients may indicate valley faults.

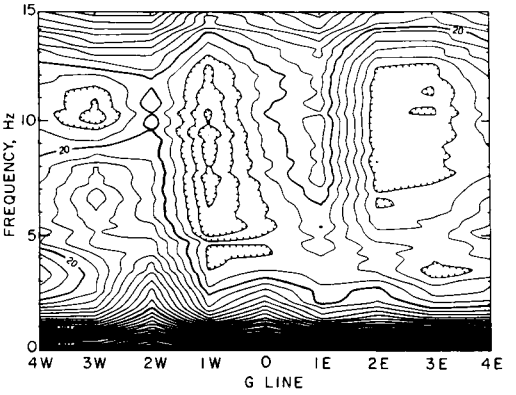


FIG. 13. Instantaneous noise field along survey line G. Abscissa is station location with 1 km spacing and ordinate is frequency. Contour interval is 2 dB. Note high wide-band noise level at valley center near 1E. Sharp gradients may indicate valley faults.

topography occurs around 2W. A remarkable feature seen in the figure is the dramatic 10 dB contrast between points 1E and 1.25E, spanning the Hot Springs fault (Figure 2). It seems the local noise field, generated by hot springs, is less attenuated east of the fault than west of it, probably due to high-$Q$ surface rocks on the east being in faulted contact with alluvium west of the fault. This geologic feature can be seen in the faults anomaly (Figure 2) as well as in the Bouguer gravity map, the $P$-wave delay profiles, and the seismic reflection section; in addition, it is indicated by surface scarps.

Asymmetrical ridges of wide-band noise with sharp gradients to the east are seen near 2W on line B (Figure 12) and near 1E on line G (Figure 13). These ridges in the noise contours, as was the case for line E, correspond in position to the location of the minimum Bouguer gravity anomaly along each line and to the location of the thickest alluvium (Beyer et al, 1976). The positions of high gradients in ground noise east of the noise ridge on line B near 2W and on line G near 1E apparently correlate with locations of shallow faults. The prominent broad peak of 6.5 to 7 Hz, seen at G3W in Figure 13, is probably also related to properties of shallow alluvium. At the south end of Grass Valley, the ground noise level is generally lower than at the north end, and this contrast is presumably due to larger distance from the Leach Hot Springs and thinner alluvial deposits to the south.

## Propagation characteristics

The most effective parameters for discriminating noise due to a buried localized source from that due to distributed surface sources and variations in local subsurface properties are the direction of propagation and the apparent phase velocity of the microseisms. Above a deeply buried source, we expect time-invariant direction of propagation associated with high-phase velocity across the array.

Time-invariant azimuths of propagating noise fields are seen at sites in the vicinity of Leach Hot Springs. Typical noise data recorded in this area show highly coherent energy, as seen in the array data from site A2N, 1 km southeast of Leach Hot Springs, shown in Figure 14. The dominant frequency of the propagating noise field in the area is 4.4 Hz. The result of $f$-$k$ analysis at the dominant frequency indicates that the noise field propagates across the array at azimuth 149 degrees, with phase velocity of 422 m/sec. The azimuth in the plot is in a direction away from the Hot Springs. In the frequency band near 2.5 Hz shown in Figure 14b, the coherent noise propagating at 904 m/sec at an azimuth of 207 degrees also is away from the Hot Springs.

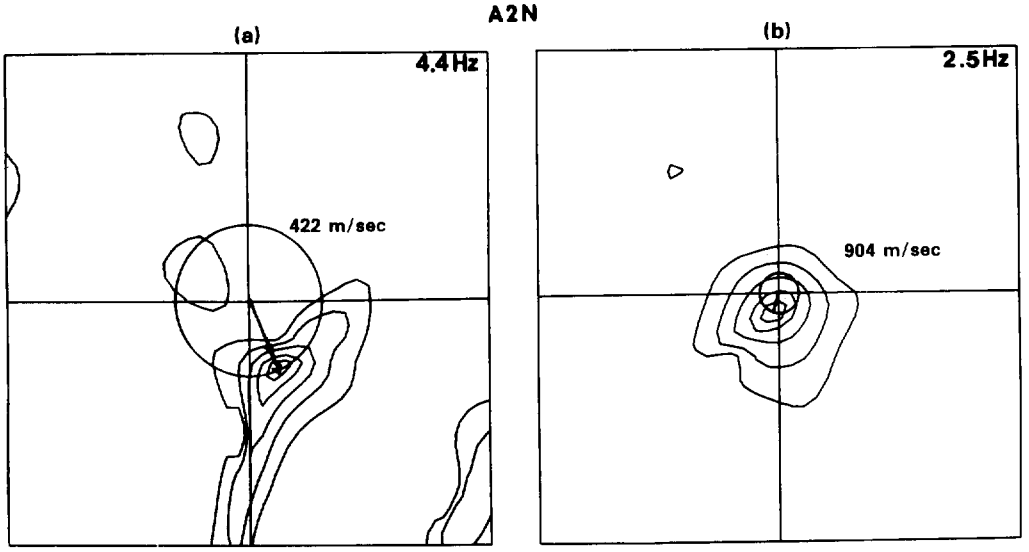


FIG. 14. High-resolution *f-k* results at site A2N, 1 km southeast of Leach Hot Springs. The microseismic field consists of (a) 4.4 Hz noise propagating in the direction 149 degrees with apparent phase velocity of 422 m/sec and (b) 2.5 Hz noise propagating in the direction 207 degrees with apparent phase velocity 904 m/sec. The maximum wavenumber plotted is 35.7 cycles/km. These noise components are apparently fundamental-mode Rayleigh waves generated at the hot springs, where near-surface velocities exceed 2.9 km/sec.

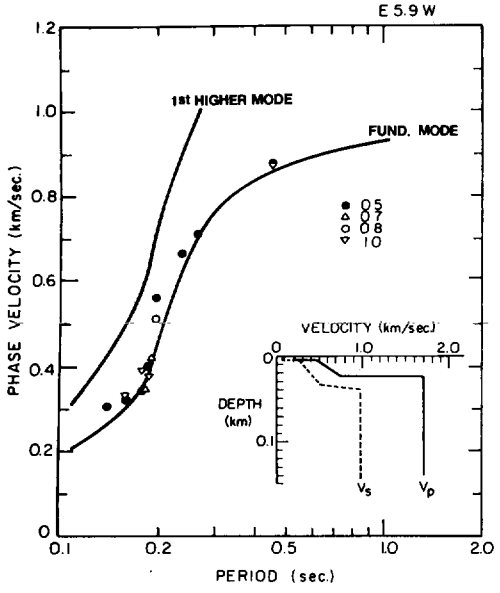


FIG. 15. Rayleigh wave dispersion curves for fundamental and first higher mode computed for the model shown, compared with observed ground noise phase velocities at site E5.9W. The observed phase velocities were determined at various times of the day by *f-k* analysis, the hour indicated by symbol type.

The noise anomaly in the center of the valley, for example, E5.9W at 5 to 7 Hz (Figure 9b), can be explained by the superposition of multipath surface waves propagating in the shallow alluvial section. The absence of a unique and time-invariant propagation direction, as seen, for example, in Figure 6a, indicates clearly that the high-amplitude ground noise at this site is not due to a local buried source. Further, the uniform propagation velocity, 340 m/sec in Figure 6a, seen at all azimuths suggests a surface wave nature of the noise field. Similar multiazimuth surface waves are seen also in the results of *f-k* analysis at 5.71 Hz for the array data at other sites. The phase velocities estimated from these plots indicate that the microseisms are apparently fundamental-mode Rayleigh waves.

## Dispersion characteristics and shallow structure

On the assumption that the microseismic field consists of surface waves, the *f-k* analysis technique allows direct measurement of the local dispersion curve by selecting phase velocities corresponding to the frequencies at peak *f-k* power spectral densities. As an example, in Figure 15 we show phase velocities so estimated, along with computed fundamental and first higher-mode Rayleigh wave dispersion curves

for a model based on $P$-wave velocities from a shallow refraction survey in the area. The effect of the very shallow velocity structure is illustrated clearly. Lateral variations in the upper 10 to 20 m will control the surface wave propagation characteristics. In estimating dispersion curves, we do not restrict sampling to the quiet periods, since larger microseisms are very coherent across the array. The dispersion measurements, besides providing local observations of phase velocity for shallow structure mapping, also provide a method of verifying the wave nature of the microseisms. It is clear that waves with periods of 1 sec and greater must be analyzed for structural information at geothermal target depths, if the microseisms are fundamental-mode Rayleigh waves (see, for example, McEvilly and Stauder, 1965).

## CONCLUSIONS

The spatial distribution of the amplitude, frequency, and wavenumber characteristics of background microseisms, or ground noise, contains information on the variation of subsurface properties and the location of buried sources of seismic waves. Extraction of the information requires careful sampling of the microseismic field in time and space. A simple field system, utilizing FM telemetry of data to a small, trailer-mounted, central recording site, was fabricated for one- or two-man installation and operation in a study of the methodology in a potential geothermal area in Grass Valley, Nevada.

Diurnal variation in the 2–20 Hz noise field is regular. A consistent diurnal variation that repeats from day to day is due apparently to meteorological and cultural sources, with typically 15 dB variation seen from the midday high noise level to the low noise level in the early morning hours of 2–4 AM. Secular variations, due to regional weather patterns, can produce a 5–10 dB range in the early morning minimum noise levels over a duration of a few days.

For spectral stability in investigating spatial variation of noise, at least 28 quiet data blocks, each 12.8 sec long, were taken simultaneously at the network stations, and the spectra were averaged for each site. This procedure produced consistent results throughout the area, revealing a characteristically low-amplitude smooth noise spectrum at hard rock sites, a prominent peak at 4–6 Hz at valley sites, and wide-band high-amplitude noise, apparently due to very shallow sources, at hot springs sites. Contour maps of noise level, normalized to a reference site, are dominated by the hot springs noise levels outlining the regions of maximum alluvium thickness. Major faults are evident when they produce a shallow lateral contrast in rock properties.

Microseisms in the 2–10 Hz band are predominantly fundamental-mode Rayleigh waves, characterized by low velocities and wavelengths as small as 20 m, requiring arrays of closely spaced geophones for adequate spatial sampling.

High-resolution $f$-$k$ processing, with proper data sampling, provides a powerful technique for mapping the phase velocity and the direction of propagation of the noise field, revealing local sources and lateral changes in shallow subsurface structure.

No evidence for a significant body wave component in the noise field was found, although it becomes clear that improper spatial sampling can give a false indication through aliasing. Noise emanating from a deep reservoir would be evident as body waves and could be traced to its source given a reasonably accurate velocity model.

## RECOMMENDATIONS

Conventional seismic ground noise surveys, conducted as outlined in this study, require a large number of stations for economical implementation. With 100 stations, for example, a week-long survey could provide maps of noise amplitude distribution, $P$-wave delay time, and microearthquake locations, as well as $f$-$k$ analyses at many sites, utilizing a 2–3 man crew. It is not clear, however, that such data will be of significant value in delineating a geothermal reservoir.

The amplitude mapping of ground noise in certain frequency bands is a poor exploration technique for delineating buried geothermal systems. The results of the amplitude mapping indicate that the amplitude variations of microseisms in an area are controlled by the near-surface geology, especially lateral variations in thickness of the alluvial layer. The large amplitude surface wave generated by surface sources and propagating horizontally will mask weak seismic waves emitted from a buried source. Therefore, amplitude mapping only reveals information on the very shallow structure.

On the other hand, the technique of $f$-$k$ analysis can, theoretically, map the wavenumber of the microseisms, discriminating the vertically incident body waves from the surface waves. The yet open question of whether a reservoir acts as a radiator of seismic body waves can be answered through careful $f$-$k$ analyses in existent geothermal areas. The array to be used for further study must be a nonaliased array of larger diameter than that used in this study. The ex-

pansion in array size will improve the resolution around the origin of the $k_x - k_y$ diagram. This improvement would provide a more accurate estimate for power at the small wavenumbers, so that the azimuth and the apparent velocity of the long-wavelength body waves are estimated more accurately. The amplitudes of body waves radiating from a source at depth are apparently much smaller than those of the ambient surface waves. In order to extract useful information from the body waves, a sophisticated signal detection and processing scheme is required. However, the *f-k* analysis technique may fail to detect the geothermal system at depth if our assumption of body wave radiation from the reservoir is not valid, or if the emanating body waves are either attenuated or completely masked by the ambient surface waves. It is fortunate that the ambient surface waves have shorter wavelengths than the anticipated body waves; because of this, the detection of weak body waves can be improved by a more sophisticated array, as is commonly done in conventional seismic reflection surveying.

If the assumption of radiated body waves is indeed valid, and if such body waves are detectable, we can trace the recorded wavefronts to their source, given a reasonably accurate velocity model. There are two schemes which have been used for projecting waves observed at the surface back into the earth and locating the source region, and these methods may be applicable to the geothermal reservoir delineation problem.

The first method is seismic ray tracing described by Julian (1970) and Engdahl and Lee (1976). If the array diameter is much smaller than the distance to the buried source, the microseismic field propagates as a plane wave across the array. Estimation of the azimuth and the apparent velocity of the propagating noise field from *f-k* analysis, along with the knowledge of the near-surface velocity distribution, can give us the incident angle of the coherent body wave noise. Given a reasonable velocity structure in the area and simultaneously occupied array sites, we can reconstruct raypaths to each site. The intersection of these raypaths indicates the region of the radiating source.

Another approach is much like that used in a conventional reflection survey with 2-D surface coverage but without a surface-controlled source. The coherent noise fields recorded by a 2-D surface array are projected downward into the assumed subsurface model. The reconstruction of the coherent noise field propagating in an upward direction can be carried out by the wave equation migration technique, using a finite-difference approximation such as the one described by Claerbout (1976). The restriction of this approach to microseismic data is that the noise field must propagate as a spherical wavefront across the geophone array. The spherical wavefront exists in the situation where the array dimension is greater than the distance to the source. In this case, we can determine the region of radiating sources in terms of the convergent pattern of the extrapolated wave fields.

It is clear that ray tracing and the wave equation migration are applicable at different source-array distances in the application of delineating geothermal reservoirs. In a practical exploration program, we do not know the depth of geothermal reservoirs, nor do we know the shape of the wavefront across the array. One way of solving the problem is to place a non-aliased array at several sites and search for the evidence of time-invariant, high-velocity body waves. As soon as the body waves are detected, one may compare several results of *f-k* analysis, using data of identical recording periods but of different sizes of subarray. The deterioration of the resolution in the *f-k* diagrams, as we expand the size of the subarray, indicates that the plane wave assumption is violated and the wavefront migration techniques should be applied. On the other hand, if the noise fields propagate as plane waves across the large array, the resolution in the *f-k* diagrams will be improved as we expand the size of subarrays, and the *f-k* analysis with seismic ray tracing is the proper technique to locate the noise source.

Based on this study, we suggest that if the geothermal system is indeed emanating detectable body waves, the analysis of ambient ground motion or seismic noise can be applied to the delineation of geothermal reservoirs. In fact, if the radiated body waves exist, the method can be one of the most effective geophysical methods in geothermal explorations. Clearly, a few carefully executed and strategically located experiments are warranted.

## ACKNOWLEDGMENTS

This study has been supported by the U. S. Energy Research and Development Administration under contract no. W-7405-ENG-48 with the Lawrence Berkeley Laboratory.

The authors are grateful to Steven Palmer, Jack Yatou, Glen Melosh, and Ernie Majer of the University of California at Berkeley and geothermal field crews of Lawrence Berkeley Laboratory for field assistance in various stages of study.

## REFERENCES


Barnard, T. E., 1969, Analytical studies of techniques for the computation of high resolution wavenumber spectra: Advanced Array Research, special report no. 9, Dallas, Texas, Texas Instruments, Inc.

Beyer, A., Dey, A., Liaw, A., Majer, E., McEvilly, T. V., Morrison, H. F., and Wollenberg, H., 1976, Geological and geophysical studies in Grass Valley, Nevada: Preliminary open file rep. LBL-5262.

Capon, J., 1969, High-resolution frequency-wavenumber spectrum analysis: Proc. IEEE, v. 57, p. 1408–1418.

Clacy, G. R. T., 1968, Geothermal ground noise amplitude and frequency spectra in New Zealand volcanic region: J. Geophys. Res., v. 73, p. 5377–5383.

Claerbout, J. F., 1976, Fundamentals of geophysical data processing: New York, McGraw-Hill Book Co., Inc., p. 184–226.

Combs, J., and Rotstein, Y., 1975, Microearthquake studies at the Coso geothermal area, China Lake, California: 2nd U.N. Symps. on the Dev. and Use of Geothermal Resources, San Francisco, p. 909–916.

Cox, H., 1973, Resolving power and sensitivity to mismatch of optimum array processors: J. Acous. Soc. of Am., v. 54, no. 3, p. 771–785.

Douze, E. J., 1967, Short-period seismic noise: SSA Bull., v. 57, p. 55–81.

Douze, E. J., and Sorrells, G. G., 1972, Geothermal ground-noise surveys: Geophysics, v. 37, p. 813–824.

Engdahl, E. R., and Lee, W. H. K., 1976, Relocation of local earthquake by seismic ray tracing: J. Geophys. Res., v. 81, p. 4400–4406.

Fix, J. E., 1972, Ambient earth motion in the period range from 0.1 to 2560 sec.: SSA Bull., v. 62, p. 1753–1760.

Goforth, T. T., Douze, E. J., and Sorrells, G. G., 1972, Seismic noise measurements in a geothermal area: Geophys. Prosp., v. 20, p. 76–82.

Guttenberg, B., 1958, Microseisms, *in* Advances in Geophysics: New York. Academic Press, v. 5, p. 53–97.

Haubrich, R. A., and Mackenzie, G. S., 1965, Earth noise 5–500 millicycles per second; 2. Reaction of the earth to oceans and the atmosphere: J. Geophys. Res., v. 70, p. 1429–1440.

Haubrich, R. A., and McCamy, K., 1969, Microseisms: Coastal and pelagic sources: Rev. of Geophys. v. 7, p. 539–571.

Iyer, H. M., 1974, Search for geothermal seismic noise in the East Mesa area, Imperial Valley, California: U.S.G.S. open-file rep. no. 74–96, 52 p.

Iyer, H. M., and Hitchcock, T., 1974, Seismic noise measurements in Yellowstone National Park: Geophysics, v. 39, p. 389–400.

——— 1976, Seismic noise survey in Long Valley, California: J. Geophys. Res., v. 81, p. 821–840.

Julian, B. R., 1970, Ray tracing in arbitrary heterogeneous media: Tech. note 1970–45, Lincoln Lab., Lexington, Mass.

Kanai, K., and Tanaka, T., 1961. On microtremors VIII: Bull. of the Earthquake Res. Inst., v. 39, p. 97–114.

Katz, L. J., 1976, Microtremor analysis of local geological conditions: SSA Bull., v. 66, p. 45–60.

Lacoss, R. T., Kelly, E. J., and Toksöz, M. N., 1969, Estimation of seismic noise structure using arrays: Geophysics, v. 34, p. 21–38.

Longuet-Higgins, M. S., 1950. A theory of the origin of microseisms: Phil. Trans. Royal Soc. London, ser. A., v. 243, p. 1–15.

Luongo, G., and Rapolla, A., 1973, Seismic noise in Lipari and Vulcano Islands, Southern Thyrrenian Sea, Italy: Geothermics, v. 38, p. 29–31.

McDonough, R. N., 1974, Maximum-entropy spatial processing of array data: Geophysics, v. 39, p. 843–851.

McEvilly, T. V., and Stauder, W. S. J., 1965, Effect of sedimentary thickness on short-period Rayleigh-wave dispersion: Geophysics, v. 30, p. 198–203.

Nicholls, H. R., and Rinehart, J. S., 1967, Geophysical study of geyser action in Yellowstone National Park: J. Geophys. Res., v. 72, p. 4651–4663.

Oliver, J., 1962, A worldwide storm of microseisms with periods of about 27 seconds: SSA Bull., v. 52, p. 507–518.

Oliver, J., and Ewing, M., 1957, Microseisms in the 11- to 18-second period range: SSA Bull., v. 47, p. 111–127.

Oliver, J., and Page, R., 1963, Concurrent storm of long and ultralong period microseisms: SSA Bull., v. 53, p. 15–26.

Robertson, H., 1965, Physical and topographic factors as related to short-period wind noise: SSA Bull., v. 55, p. 863–877.

Sass, J. H., Lachenbruch, A. H., Monroe, R. J., Greene, G. W., and Moses, T. H., 1971, Heat flow in the western United States: J. Geophys. Res., v. 76, p. 6376–6413.

Savino, J., McCamy, K., and Hade, G., 1972, Structures in earth noise beyond twenty seconds—a window for earthquakes: SSA Bull., v. 62, p. 141–176.

Sax, R. L., and Hartenberger, R. A., 1965, Seismic noise attenuation in unconsolidated material: Geophysics, v. 30, p. 609–615.

Sorrells, G. G., McDonald, J. A., Der, Z. A., and Herrin, E., 1971, Earth motion caused by local atmospheric pressure changes: Geophys. J. R. Astr. Soc., v. 26, p. 83–98.

Whiteford, P. C., 1970, Ground movement in the Waiotapu geothermal region, New Zealand: Geothermics, special issue on proceedings of the U.N. Symps. Dev. Util. of Geothermal Resources, 2, part III, p. 478–486.

——— 1975, Studies of the propagation and source locations of geothermal seismic noise: 2nd U.N. Symps. on the Dev. and Use of Geothermal Resources, San Francisco, p. 1263–1271.

Wilson, C. D. V., 1953, The origins and nature of microseisms in the frequency range 4 to 100 c/s: Proc. R. Soc. A., v. 217, p. 176–202.